MNRAS 000, 1–11 (2019) Preprint 26 May 2021 Compiled using MNRAS LATEX style file v3.0

The SAMI galaxy survey: the stellar metallicity-gravitational potential relation and its constraints on galaxy quenching

Sam P. Vaughan,[1,2], Tania M. Barone, Scott Croom, Luca Cortese and the SAMI team ⋆
[1]Sydney Institute for Astronomy, School of Physics, Building A28, The University of Sydney, NSW 2006, Australia
[2]ARC Centre of Excellence for All Sky Astrophysics in 3 Dimensions (ASTRO3D), Australia

Accepted XXX. Received YYY; in original form ZZZ

ABSTRACT

In this work, we investigate how the central stellar metallicity ([Z/H]) of 1902 galaxies from the SAMI galaxy survey is related to their stellar mass, M_*, and gravitational potential, $\Phi = \log_{10}\left(\frac{M_*}{M_\odot}\right) - \log_{10}\left(\frac{r_e}{\mathrm{kpc}}\right)$. In agreement with previous studies, we find that passive and star-forming galaxies occupy different areas of the [Z-H]-M_* plane, with passive galaxies having higher stellar metallicity than star-forming galaxies at fixed mass. When investigating the relationship with Φ, however, we find that galaxies lie on the same relation between [Z/H] and Φ regardless of star-formation rate, with a scatter of only 0.15 dex. We use the [Z-H]-M_* and [Z/H]-Φ relations to constrain possible evolution in the mass-size plane, and build a simple toy model of galaxy evolution to explain and understand our results. We are able to reproduce an offset in stellar metallicity between passive and star-forming galaxies at fixed mass with a model containing instantaneous quenching, if the probability that this quenching happens depends on both a galaxy's mass and size. We therefore conclude that such a difference in metallicity cannot by itself be used as evidence of slow quenching processes, in contrast to previous studies. We build on previous work to reiterate that the size of galaxies is an essential quantity to consider when studying their stellar populations, and discuss how the [Z/H]-Φ relation from this work may be used to infer stellar metallicities in large photometric studies without the need for expensive spectroscopic observations.

Key words: keyword1 – keyword2 – keyword3

1 INTRODUCTION

Galaxies in the Universe can broadly be classified into two categories: those which are currently forming stars and those which are not. Understanding and quantifying exactly which physical processes play a role in shaping this dichotomy is a fundamental goal of galaxy evolution, but despite decades of work on the topic (e.g. Tinsley 1968; Larson et al. 1980; Dekel & Birnboim 2006; Peng et al. 2010; Schawinski et al. 2014, among many others) a complete picture remains out of reach.

In the most popular framework for discussing the life cycles of galaxies, the idea of star formation "quenching" plays a central role. This model envisions that the natural state of a galaxy is to be forming stars at a rate which places it on the "Main-Sequence" of star-formation (Noeske et al. 2007; Speagle et al. 2014; Renzini & Peng 2015). Internal or external process then act to stop the galaxy's star formation, causing it transition off the Main Sequence and join the passive population. The question of "what leads to the division in galaxy properties?" can then be reframed to instead ask "what causes quenching?". A wide range of physical drivers of have been proposed and investigated, including feedback from a galaxy's central black hole (Silk & Rees 1998; Magorrian et al. 1998; Di Matteo et al. 2005), the effects of falling into a massive galaxy cluster (Gunn & Gott 1972; Abadi et al. 1999), the secular evolution of stellar orbits over cosmic time (Kormendy & Kennicutt 2004; Sellwood 2014) and the occurrence of "compaction" events which increase a galaxy's central surface density (e.g. Sellwood Woo; Woo & Ellison 2019).

Finding direct evidence of quenching in an individual object by catching such processes in the act is notoriously difficult, however, since we lack the ability to study individual galaxies across cosmic time. Another route to approach the problem is by studying a large sample of galaxies and investigating the properties of the entire population as a whole. This was the approach taken by Peng et al. (2015, hereafter P15) and Trussler et al. (2020, hereafter T20), who used the stellar ages and metallicities of tens of thousands of galaxies from the Sloan Digital Sky Survey (SDSS; York et al. 2000; Eisenstein et al. 2011; Blanton et al. 2017) in the nearby Universe to conclude that quenching processes must be slow in nature, with a quenching timescale on the order of 4 Gyrs.

Key to their conclusions is the correlation between stellar mass and stellar metallicity, and the fact that quiescent galaxies tend to be more metal rich than star forming galaxies at fixed mass (P15; T20). Previous studies have discussed that the size of a galaxy is also an important parameter to consider when analysing its stellar populations (e.g. McDermid et al. 2015; Scott et al. 2017), however, and recent work by Barone et al. (2018), D'Eugenio et al. (2018) and Barone et al. (2020) has quantified this fact: they find that the metallicity of gas and stars in galaxies forms a tighter relationship with a galaxy's gravitational potential ($\Phi \sim M_*/r$) compared to the relationship between metallicity and stellar mass alone. Their work

⋆ Contact e-mail: sam.vaughan@sydney.edu.au (SPV)

begs the question of whether the difference in metallicity between passive and star-forming galaxies at fixed stellar mass discussed by P15 and T20 is still evident at fixed gravitational potential. Can quenching processes which depend on both mass *and size* be used to explain the diversity of galaxies we observe today in the local Universe?

In this work, we build on the previous studies of Barone et al. (2018); D'Eugenio et al. (2018) and Barone et al. (2020) and, for the first time, investigate the correlations between stellar metallicity, stellar mass and gravitational potential for a homogeneously-observed sample containing both quiescent and star-forming galaxies (instead of studying each class of galaxy separately). We then ask a similar question to P15 and T20: what can we learn about the quenching timescales of galaxies from these observations? One key difference between our sample and that of P15 and T20 is that each galaxy we study has a robust half-light radius measurement, allowing us to investigate the roles of mass and size in regulating galaxy quenching processes.

The outline of this paper is as follows. In Section 2 we describe our sample of galaxies and briefly outline our method for measuring stellar metallicities. In Section 3 we present our results and in Section 4 we discuss our findings, introducing a simple toy model of galaxy quenching to reproduce the population of local galaxies in Section 4.3. In Section 5 we draw our conclusions. We assume a flat Λ cold dark matter (ΛCDM) cosmolgy with $\Omega_\Lambda = 0.7$, $\Omega_M = 0.3$, and $H_0 = 70 \mathrm{kms}^{-1}\mathrm{Mpc}^{-1}$. We also assume a Chabrier (2003) initial mass function where necessary.

2 STELLAR POPULATION MEASUREMENTS AND ANCILLARY DATA

The galaxies in our sample are drawn from data release 3 (DR3) of the SAMI galaxy survey (Croom et al. 2021). SAMI DR3 provides fully reduced datacubes for 3068 galaxies in the local Universe, selected to have a redshift (z) less than 0.11 and a stellar mass between $7.8 \leq \log_{10}(\mathrm{M}_*/\mathrm{M}_\odot) \leq 11.8$. The SAMI instrument (Croom et al. 2012) is mounted at the prime focus on the Anglo-Australian Telescope that provides a 1 degree diameter field of view. SAMI uses 13 fused fibre bundles (Hexabundles,Bland-Hawthorn et al. 2011; Bryant et al. 2011 with a high (75%) fill factor. Each bundle contains 61 fibres of 1.6″diameter resulting in each IFU having a diameter of 15″. The IFUs, as well as 26 sky fibres, are plugged into pre-drilled plates using magnetic connectors. SAMI fibres are fed to the double-beam AAOmega spectrograph (Sharp et al. 2006). AAOmega allows a range of different resolutions and wavelength ranges. The SAMI Galaxy survey uses the 570V grating at 3700-5700Å giving a resolution of $R = 1730$ ($\sigma = 74$ km s^{-1}), and the R1000 grating from 6250-7350Å giving a resolution of $R = 4500$ ($\sigma = 29$ km s^{-1}).

We measure stellar population parameters as a function of radius for each galaxy in the sample. A full description of these measurements used in this work will be presented in a forthcoming paper (Vaughan et al. in prep). We give a brief summary here. Firstly, the blue and red arm spectra are joined together and convolved with a Gaussian kernel (of variable width) such that the spectral resolution is a constant value at all wavelengths. We then use the Voronoi binning algorithm of Cappellari & Copin (2003) to aggregate spectra together such that their combined spectrum has a minimum signal-to-noise (S/N) ratio of 20 Å^{-1} in the V-band. Individual spaxels with a S/N above 20 Å^{-1} are left unbinned. 181 galaxies lacked the required S/N to create a single Voronoi bin and were discarded. In total, our sample contains 81,087 individual Voronoi bins from 2887 galaxies.

We then use the penalised-pixel fitting code `pPXF` (Cappellari & Emsellem 2004; Cappellari 2017) to fit the simple stellar population (SSP) models of (Vazdekis et al. 2015) to the spectrum from each Voronoi bin. In essence, `pPXF` finds the weighted sum of SSP templates which best recovers the input galaxy spectrum. We also include gas emission line templates corresponding to the Balmer series (Hα Hβ and Hγ) as well as the atomic species [NII], [OIII], [SII], and [OI]. We also use a multiplicative Legendre polynomial of order 10 to correct for small differences in the shape of the observed and template spectra. We perform the analysis twice, firstly with the SSP spectra normalised such that the resulting stellar population parameters are light-weighted and then again with the SSP spectra normalised such that the results are mass-weighted.

For each Voronoi bin, we record the best-fit weighted average stellar age and stellar metallicity (for both light-weighted and mass-weighted quantities). At this stage, we remove from our sample any galaxies which have fewer than four independent Voronoi bins or have $\log_{10}(\mathrm{M}_*/\mathrm{M}_\odot) < 8$. This leaves us with 79,326 spectra from 1902 galaxies, which we call the "full sample". For every galaxy in the full sample, we then infer the stellar metallicity at the very centre of the galaxy (galacto-centric radius $r = 0$) by fitting a straight line to the stellar age and metallicity measurements as a function of radius. We perform this fit to all galaxies in the full sample simultaneously by building a hierarchical Bayesian model, but have also ensured that our results are unchanged if we simply fit the measurements as a function of radius for each galaxy independently in the standard manner (see Vaughan et al. in prep for details). For each galaxy in the full sample we are therefore left with eight measurements: the age and metallicity gradients and the central ages and metallicities for both light-weighted and mass-weighted quantities. This paper is only concerned with the mass-weighted central stellar metallicity values of each galaxy; the remaining measurements are fully discussed in Vaughan et al. (in prep).

For each galaxy, we also require a number of ancillary measurements for our analysis. Stellar masses for each SAMI galaxy were derived using the prescription of Taylor et al. (2011). Total star formation rates (SFRs) were derived from Hα flux measurements by Medling et al. (2018), with an aperture correction applied where appropriate. Finally, half-light radii were measured using the Multi-Gaussian expansion method of Cappellari (2002) from high-resolution r-band images of each object (D'Eugenio et al. 2021).

Finally, we also create a "central-only sample" by using the Galaxy and Mass Assembly (GAMA) galaxy group catalogue (G^{3}C) of Robotham et al. (2011) to differentiate between galaxies which are the most massive object in their dark matter halos ("centrals") and those which are not ("satellites"). The goal of the central-only sample is to create a sample of objects which have primarily undergone (or will undergo) *internal* quenching processes (in contrast to quenching processes which depend on environment, which predominantly influence satellite galaxies: see e.g. Woo et al. 2017). We will use this sample to compare to the quenching toy model presented in 4.3, since the model does not include any prescription for environmental quenching.

Plots of the mass-size and mass-SFR planes for the SAMI parent catalogue and our samples are shown in Figure 1.

3 RESULTS

The main results of this work concentrate on the relationship between the central metallicity of galaxies and their gravitational potential, and are presented in Figure 2.

Figure 1. The mass-size plane (left) and mass-SFR plane(right) of our sample. Each panel shows the parent SAMI catalogue (black), the galaxies which form our "full" sample (orange) and those which are part of the "centrals-only" sample (green). Histograms show the marginal distribution of each parameter. In the mass-SFR plane, we also show the star formation rate "main sequence" from Renzini & Peng (2015) which we use to classify galaxies as star-forming, passive or intermediate: star-forming galaxies are above the highest dotted line; quenched galaxies are below the lower dotted line; intermediate galaxies are between the dotted lines.

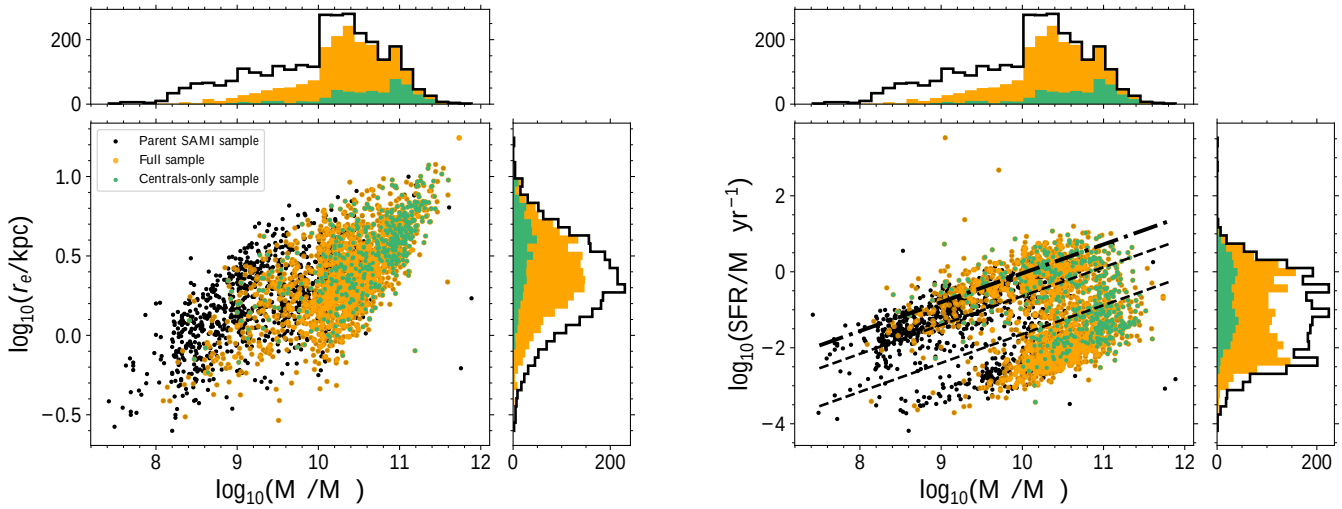

Firstly, we classify galaxies as being star-forming or passive using simple cuts in the mass-SFR plane. Following Renzini & Peng (2015), we define the star-forming "main sequence" to be

$$\log(\mathrm{SFR}) = 0.76\log(\mathrm{M_*/M_\odot}) - 7.64 \quad (1)$$

with a scatter around the relation of 0.3 dex. By finding the difference between a galaxy's measured star-formation rate (SFR) and the SFR of a galaxy of the same mass on the main sequence ($\Delta\mathrm{SFR_{MS}}$), we separate galaxies into star-forming, intermediate (or "green-valley") or passive in the following manner:

$$\mathrm{SF\,galaxies} : \Delta\mathrm{SFR_{MS}} > -0.6 \quad (2)$$

$$\mathrm{Green-valley\,galaxies} : -0.6 \leq \Delta\mathrm{SFR_{MS}} \leq -1.6 \quad (3)$$

$$\mathrm{Passive\,galaxies} : \Delta\mathrm{SFR_{MS}} < -1.6 \quad (4)$$

In essence, we define star-forming galaxies to be within 2σ (0.6 dex) of the main sequence; passive galaxies to be more than 5σ from the main sequence (1.6 dex); and intermediate galaxies to fall between these two categories. Reasonable changes to these values have no effect on our conclusions. Our full sample consists of 682 star-forming galaxies, 903 passive galaxies and 317 intermediate galaxies.

We then show the results of our metallicity measurements as a function of mass in the left hand panel of Figure 2, with SF galaxies coloured blue, passive galaxies shown in red and intermediate galaxies in yellow. Quantitative results of fitting a straight line to the star-forming and passive galaxies are shown in Table 1.

We confirm the well known result that passive and SF galaxies occupy different areas of the mass-metallicity plane, and that passive galaxies tend to be more metal-rich than SF galaxies at the same mass. The straight line fits to the mass-metallicity relation are in excellent agreement with the recent work of T20 and P15; like T20, we find that, at a stellar mass of $\log(\mathrm{M_*/M_\odot}) = 10.3$, the offset in metallicity between star-forming and passive galaxies is 0.18 dex. We also find that this difference in metallicity between star-forming and passive galaxies is mass dependent, dropping to become negligible at the high-mass end of our sample. Phrased another way, the stellar mass of a galaxy is not enough on its own to predict its stellar metallicity; its star-formation rate is also required.

The main new result of this work is shown in the right hand panel of Figure 2, where we plot the mass-weighted central metallicity of each galaxy against its gravitational potential, Φ, where $\Phi = \log_{10}\left(\frac{M_*}{M_\odot}\right) - \log_{10}\left(\frac{r_e}{\mathrm{kpc}}\right)$. This plot shows that the metallicity difference between the average star-forming and passive galaxy at fixed potential, rather than fixed mass, is much smaller. As first discussed in Barone et al. (2018, 2020), stellar metallicity correlates much better with gravitational potential than mass (as quantified by the intrinsic scatter around the relation). Here, we show for the first time that the distributions of star-forming and passive galaxies in the metallicity-potential plane smoothly follow on from one another, implying that knowing a galaxy's potential is sufficient to infer its stellar metallicity *without knowing whether a galaxy is passive or star-forming*.

We show the best fit [Z/H]-Φ relation for all galaxies combined in Table 1, and measure the standard deviation of the residuals around this relation to be 0.16 dex. The six prominent outliers in Figure 2 at low metallicity all have high quality observations, containing between 9 and 90 independent Voronoi bins each. Five of these outliers show very low mass-weighted metallicity in their central regions combined with higher metallicity outskirts, implying interesting formation histories; perhaps a sustained period of accretion of low metallicity gas fuelling central star-formation. For the sixth, we measure low metallicity at all radii. We note that removing these six galaxies from the residuals decreases the 1-σ scatter around the best-fit relation to 0.12 dex.

4 DISCUSSION

Many previous studies have discussed the correlations between a galaxy's stellar metallicity and its structural parameters, although

Figure 2. Mass-metallicity (left) and gravitational potential-metallicity (right) relations for our SAMI galaxies. We separate our sample into passive, star-forming and intermediate ("green valley") galaxies according to the definition in Renzini & Peng (2015). Outlying points are indicated by downward arrows. Dotted lines show a straight line fit to the the passive and star-forming populations separately. The dot-dash lines shows a fit to all galaxies at once. The lower panels show the residuals around the dot-dash lines as a function of stellar mass (left) and gravitational potential (right). The standard deviation of the residuals around the fit to the Φ-[Z.H] relation is 0.15 dex, but this value is inflated by six outlying points; excluding these gives a more Gaussian distribution of $\sigma = 0.12$ dex. The offset between passive and star-forming galaxies in the mass-metallicity plane is almost identical to that measured in Trussler et al. (2020) and Peng et al. (2015). The main result of this work is the right hand panel, which shows that all galaxies form a single sequence in the gravitational potential-metallicity plane, regardless of their star-formation rate.

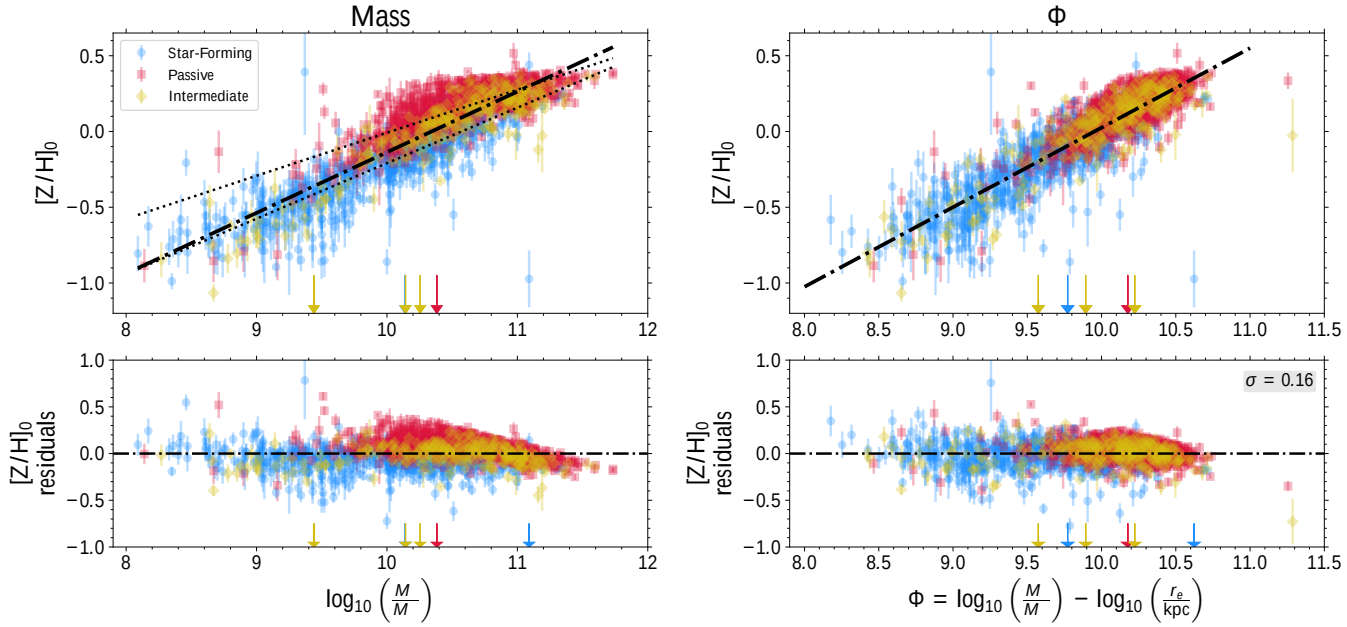

Table 1. Results from the straight line fits to the mass-metallicity and potential-metallicity planes for star-forming, passive and intermediate ('green valley') galaxies. We fit relations of the form $[Z/H] = m(\log_{10}(M_*/M_\odot) - 10.3) + c$ for the mass-metallicity plane and $[Z/H] = m(\log_{10}(M_*/M_\odot) - \log_{10}(r_e/\mathrm{kpc}) - 10.0) + c$ for the mass-potential plane. The difference in metallicity between galaxies at fixed mass is in very good agreement with Peng et al. (2015) and Trussler et al. (2020).

	Mass		Potential	
	m	c	m	c
Star-forming	0.37 ± 0.01	-0.10 ± 0.01	0.48 ± 0.01	-0.02 ± 0.01
Passive	0.28 ± 0.01	0.08 ± 0.01	0.45 ± 0.01	0.06 ± 0.01
Intermediate	0.42 ± 0.02	-0.05 ± 0.01	0.53 ± 0.02	0.01 ± 0.01
Combined	0.40 ± 0.01	-0.02 ± 0.01	0.53 ± 0.01	0.03 ± 0.01

predominantly in terms of velocity dispersion σ (e.g. Trager et al. 2000; Thomas et al. 2005; Nelan et al. 2005; Graves et al. 2009a,b; McDermid et al. 2015; Scott et al. 2017) rather than gravitational potential as in this work.

The two quantities are obviously closely related; assuming galaxies are virialsed, $\sigma^2 \propto M/R$. We show this relationship between central velocity dispersion, σ, and Φ for the full sample in Figure 3, which clearly shows the expected linear correlation for galaxies with σ greater than the SAMI instrumental resolution (of ≈ 50 kms^{-1}). We prefer to use the gravitational potential in this work to allow us to extend Figure 2 to the lowest values of Φ in our sample, without the complication of measuring velocity dispersion values close to (or below) the instrumental resolution.

Barone et al. (2018) and Barone et al. (2020) were the first to show quantitatively that stellar metallicities correlated tightly with the purely photometric quantity $\Phi \sim M/r_e$, and that this correlation was tighter than for stellar mass alone. Their work concentrated first on early-type galaxies and then on star-forming galaxies, however, without drawing conclusions about a combined sample. Here, we show for the first time that star-forming, intermediate and quiescent galaxies all lie on the same relation in the [Z/H]-Φ plane.

The physical mechanism which drives this relation is not yet fully understood, but is likely due to the relationship between gravitational potential and the local escape velocity of the system (e.g. Franx & Illingworth 1990; Scott et al. 2009, 2017). Galaxies with deeper potential wells are more able to retain the metal-rich winds and ejecta from massive stars which pollute their interstellar media, meaning that their future generations of stars will be more metal rich than those in galaxies with shallower potential wells.

The fact that galaxies in our sample follow a single [Z/H]-Φ relation has interesting implications for large photometric surveys of galaxies. Section 3 shows that stellar metallicity can be determined solely from photometric observations of r_e and M_* to a 1-σ accuracy of ≈ 0.15 dex, regardless of the galaxy's star-formation rate.

To date, estimating stellar metallicities without spectroscopic information, using broad-band colours or via panchomratic spectral energy distribution (SED) fitting, is notoriously unreliable. Many SED fitting codes therefore treat stellar metallicity as a nuisance parameter or fix it at solar metallicity (e.g. Skelton et al. 2014, and see the discussion in Conroy 2013). Other studies have shown that the choice of different stellar population synthesis models gives different results for the same input colours (Lee et al. 2007; Eminian et al. 2008; Conroy 2013).

Stellar masses, on the other hand, are much more straightforward

Figure 3. The logarithm of the velocity dispersion of the central Voronoi bin (σ_0) for each galaxy against the galaxy's gravitational potential, $\Phi = \log_{10}\left(\frac{M_*}{M_\odot}\right) - \log_{10}\left(\frac{r_e}{\mathrm{kpc}}\right)$. The expected linear relationship is clear for galaxies with σ_0 above the SAMI instrumental resolution of ≈ 50 kms^{-1}.

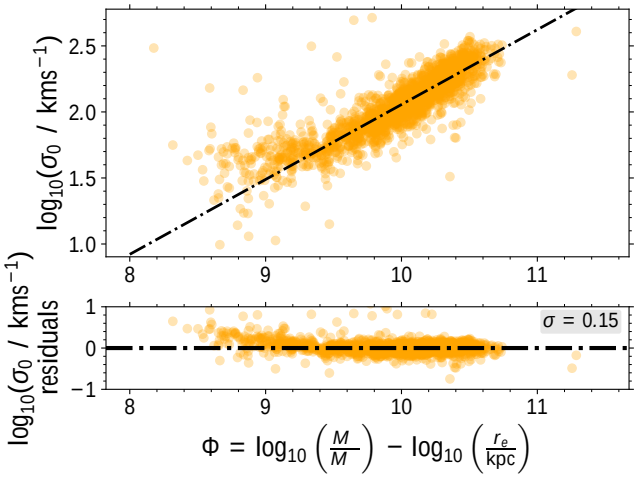

and robust outputs of SED fitting (due to the fortuitous degeneracies which exist between dust, age, and metallicity: Bell & de Jong 2001; Taylor et al. 2011). The [Z/H]-Φ relation could therefore allow for the estimation of stellar metallicities for large catalogues of galaxies without expensive spectroscopic observations for the first time. Furthermore, whilst the correlation in Figure 2 has till now only been investigated in the low-redshift Universe, further work calibrating this relationship at higher redshift could allow for studies of stellar metallicity over cosmic time (and see also Barone et al. in prep).

4.1 Implications for galaxy quenching

T20 and P15 use the difference in metallicity between star-forming and passive galaxies at $z = 0$ to conclude that most galaxies in the Universe undergo slow quenching ("starvation"). Their argument is as follows. During the course of stellar evolution, the stars in a galaxy will convert hydrogen and helium into more complex elements. A fraction of the stars in a galaxy will return their metal content to the interstellar medium (through supernovae or mass-loss from stellar winds), which increases the galaxy's overall gas-phase metallicity. On the other hand, accretion of pristine gas from the galaxy's halo or cosmic filaments will tend to dilute a galaxy's gas reservoir and lower its metallicity. The balance of these two processes sets whether a galaxy's next generation of stars will tend to have a lower, higher or similar stellar metallicity to previous generations.

If a galaxy's supply of cold gas is quickly removed or star formation is quickly suppressed, both of these processes are stopped and the stellar metallicity of a galaxy after quenching is the same as when quenching started. However, if star formation in the disc of a galaxy is allowed to continue but accretion of low-metallicity gas is cut off- i.e. the quenching is slow- this balance is upset and the galaxy's gas-phase metallicity is no longer being diluted. Generations of stars formed during slow quenching will be of a higher metallicity than before, and this process continues until the galaxy's gas is exhausted. Under this scenario, the galaxy's stellar metallicity is much higher after quenching than it was before.

T20 and P15 argue that galaxies evolve along the "main sequence" in the SFR-M$_*$ plane and the star forming mass-metallicity relation until slow quenching begins. During quenching, their SFR decreases and their metallicity increases such that they eventually lie in the passive regions of the main sequence and the mass-metallicity relations. This evolution leads to vertical or nearly vertical tracks in the mass-metallicity plane, as a large increase in metallicity is accompanied by only a small increase in stellar mass (P15; T20).

Our findings of a single [Z/H]-Φ relation for all galaxies, regardless of star-formation rate, raises questions for this interpretation. Firstly, Figure 2 shows the importance of having robust size measurements for each galaxy. The near vertical motion in the mass-metallicity plane proposed by P15 and T20 must *also* be accompanied by a decrease in size for the galaxy undergoing quenching to remain on the [Z/H]-Φ plot from Figure 2.

For an increase in metallicity of 0.2 dex and no change in stellar mass, the straight-line fit from Table 1 implies that the potential of the galaxy must change by $\approx$0.4 dex. For no change in stellar mass, the half-light radius of a galaxy must therefore *decrease* by 0.4 dex (i.e. end up at $\sim$40% of its value before quenching began). Such a reduction in size is not found in simulations of individual galaxies undergoing quenching (e.g. Genel et al. 2018), nor in the recent study of Croom et al. 2021 who investigated the effects of disk-fading on star-forming galaxies and found a reduction in r_e of $\approx$ 10% (0.05 dex). Moreover, a number of studies have found that recently quenched galaxies tend to have large radii (i.e. radii similar to star-forming galaxies) when they join the passive population (so called "progenitor bias": e.g. Cassata et al. 2013; Carollo et al. 2013; Krogager et al. 2014).

We note that a key assumption underlying the argument of P15 and T20 is that today's star-forming galaxies will end up evolving into (i.e. occupying the same locus of points in the mass-metallicity plane as) today's quiescent galaxies. Whilst an appealing picture, this is not necessarily the case. As discussed succinctly in Abramson et al. (2016), it should be emphasised that *none* of the star-forming galaxies in Figure 2 are the progenitors of the quiescent galaxies in Figure 2; discussing *evolutionary* tracks in *cross-sectional* snapshots of the Universe is fraught with difficulty.

4.2 Evolution in the mass-size plane

Our investigation of the mass-metallicity and potential-metallicity planes allow us to constrain the ways in which galaxies evolve in the mass-size plane as their stellar mass and radius increase. In order for both the mass-metallicity and potential-metallicity relations to be as tight as observed, the evolution of a galaxy's gravitational potential (and hence its growth in size as it grows in mass) can be inferred. Here we make two important assumptions: that galaxies evolve along the [Z/H]-Φ and [Z/H]-M$_*$ relations from Figure 2; and that the slopes of these two relationships are unchanged over cosmic time.

This second assumption needs to be tested, by measuring Φ and central stellar metallicity for galaxies at high redshift (e.g. see Barone et al. 2021 in prep and the forthcoming MAGPI survey; Foster et al. 2020). However, the fact that galaxies which are currently star-forming follow the same [Z/H]-Φ relation as those which quenched at higher redshift implies that this assumption is reasonable.

We now use the straight line fits from Section 3 to measure the rate of change of [Z/H] in terms of both $\log_{10}(\mathrm{M}_*/\mathrm{M}_\odot)$ and $\log_{10}(\Phi/\mathrm{M}_\odot\mathrm{kpc}^{-1})$. We label these gradients m_{M_*} and m_Φ respectively. We have that

$$m_\Phi = \frac{d[\mathrm{Z/H}]}{d\log(\Phi)} = \frac{d[\mathrm{Z/H}]}{d\log(M_*)}\frac{d\log(M_*)}{d\log(\Phi)} = m_{M_*}\frac{d\log(M_*)}{d\log(\Phi)} \quad (5)$$

and since $\log(\Phi) = \log(M_*) - \log(r)$, we have that $\frac{d\log(M_*)}{d\log(\Phi)} = (1 - \frac{d\log(r)}{d\log(M_*)})^{-1}$. Therefore

$$\frac{d\log(r)}{d\log(M_*)} = 1 - \frac{m_{M_*}}{m_\Phi} \quad (6)$$

This means that galaxies must evolve in size according to Equation 6, and we can estimate these values using our fits to Figure 2. We find that for star-forming galaxies $\Delta\log_{10}(r/\mathrm{kpc}) = 0.24 \pm 0.03\Delta\log_{10}(M_*/M_\odot)$. For quiescent galaxies, $\Delta\log_{10}(r/\mathrm{kpc}) = 0.37 \pm 0.03\Delta\log_{10}(M_*/M_\odot)$.

The evolution of star-forming galaxies in the mass-size plane as they accrete gas and grow in mass and size can be modelled as a power law, $\Delta\log_{10}(r/\mathrm{kpc}) \sim \alpha\Delta\log_{10}(M_*/M_\odot)$. Our result for star-forming galaxies is remarkably close to the slope of the mass-size relation from van der Wel et al. (2014) for galaxies between $0.25 < z < 3$, who find $\alpha \approx 0.25$. Further recent studies have inferred $\alpha \approx 0.3$ from observations (van Dokkum et al. 2013) and simulations (Zolotov et al. 2015), with other studies finding $\alpha \approx 0.4$ (Hirschmann et al. 2013) and $\alpha \approx 0.15$ (Genel et al. 2018).

On the other hand, the result for quiescent galaxies is much shallower than the observed mass-size relation for passive objects (0.37 ± 0.03 rather than ≈ 0.75 from van der Wel et al. 2014 or $\approx$0.5 from Mowla et al. 2019). We take this as evidence that our assumption that galaxies evolve along the [Z/H]-Φ and [Z/H]-M_* relations is not true for passive galaxies, and that their evolution in mass and size is decoupled from their [Z/H].

We note that we do not expect the central metallicity of passive galaxies to vary much over time, since no new stars are being formed. In fact, the mass and size evolution of passive galaxies becomes dominated by major or minor mergers with the stellar population simply evolving passively (the so-called "two-stage" evolution of passive galaxies: e.g. Naab et al. 2009; Oser et al. 2010). Instead, the majority of accreted matter is deposited at large radii, which leads to steep tracks in the mass-size plane (e.g. van Dokkum et al. 2010) but little influence on the central stellar populations (see Cappellari 2016 for a discussion).

Whilst this evolution in the mass-size plane will influence the value of Φ we measure, we note that major mergers with size growth proportional to mass growth ($\alpha \approx 1$) will leave the measured gravitational potential unchanged. Any evolution with a steeper mass-size dependence (e.g. such as minor mergers with $\alpha \approx 2$, as discussed in van Dokkum et al. 2010), combined with no change in [Z/H] will push passive objects to the left of the [Z/H]-Φ locus. The fact that passive galaxies tend to follow the same relation as star-forming galaxies, however, may imply that most of their mass-size evolution has been along tracks where $\alpha \approx 1$.

A simple test for this behaviour would be to investigate any residual trend in the [Z/H]-Φ relation with the redshift at which each passive galaxy in our sample quenched (measured by investigating their star-formation histories). Under the assumption that galaxies which quenched at high redshift are more likely to have undergone one or several major mergers (with $\Delta\log_{10}(r/\mathrm{kpc}) \sim 2\Delta\log_{10}(M_*/M_\odot)$), these objects should preferentially lie to the left of the passive sample.

4.3 Quenching toy models

We now investigate whether we can reproduce our observations using toy models of galaxy quenching. The aim of this Section is to investigate whether a model with almost instantaneous quenching- rather than the slow quenching advocated by P15 and T20- can simultaneously account for the distribution of galaxies in the mass-metallicity, potential-metallicity and mass-size planes.

Figure 4. The mass-size plane of the central galaxies in our sample. Star-forming galaxies are shown in blue and quenched galaxies are shown in red. The grey shaded region bounded by the dot-dashed lines show the regions of the diagram where we assign galaxies a non-zero probability of quenching during their next timestep. This region is comprised of a line of fixed surface density (shallow dotted line) and a line of fixed gravitational potential (steep dotted line).

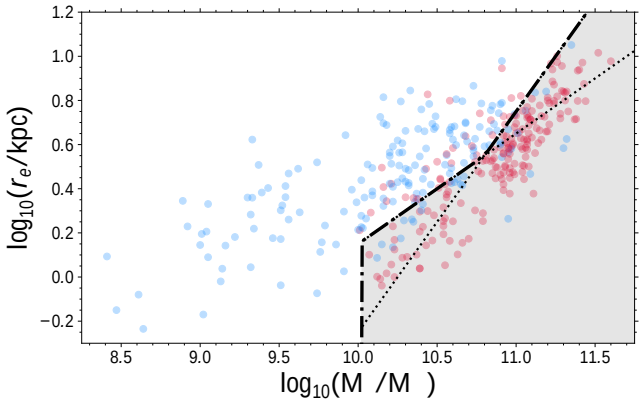

We build a simple model where star-forming galaxies grow in mass and size and evolve in metallicity as they accrete gas and form new stars. These galaxies then have a probability to quench at the start of each timestep, with this probability (p_q) depending on a combination of their mass and their size. Once galaxies become quenched, they stop their evolution and fix their values of mass, size and metallicity until redshift 0.

We begin by assigning a formation redshift to each galaxy, which is drawn from a uniform distribution between one and six. We next assign galaxies a stellar mass. We use the results from Davidzon et al. (2017), who study the galaxy stellar mass function of star-forming and passive galaxies out to redshift six. We use the results from their "active sample" to draw stellar masses from a double Schechter function at $z \leq 3$ and a single Schecter function at $z > 3$.

We then place galaxies on the mass-size relation for star-forming galaxies at the redshift of their formation, using measurements from van der Wel et al. (2014). Next, we must assign each galaxy a stellar metallicity. Measurements of the mass-metallicity relation at high redshift are currently limited to studies of ionised gas emission lines. We therefore make a further assumption; that the slope of the gravitational potential-stellar metallicity relationship is the same at high-redshift as it is at low redshift (i.e. that measured in Section 3).

We are then left with two free parameters; the intercept of this relationship and the intrinsic scatter around the relation. We choose an intercept of 0.03 dex to match the "combined" relation from Table 1, and an intrinsic scatter of 0.08 dex.

Galaxies are evolved forward in time using a timestep of 100 Myr, from their formation redshift to today. To set the amount of stellar mass formed at each timestep, we place star-forming galaxies on the main sequence of star-formation at the appropriate redshift, using the "consensus" relation from Speagle et al. (2014). Furthermore, galaxies grow in size and metallicity according to the following expressions:

Figure 5. A comparison between the data from our sample of SAMI central galaxies (top row) to simulated galaxies from our toy model of instantaneous quenching (bottom row). The columns show the [Z-H]-M_* relation (left), the [Z-H]-Φ relation (middle) and the mass-size relation (right). We find a very good quantitative agreement between the two samples; in particular, we recover an offset between the metallicities of star-forming and passive galaxies at M_*=10.5 of ≈ 0.17 dex, the same value we observe for the SAMI centrals. This implies that the difference in metallicity between star-forming and passive galaxies at fixed mass cannot, in isolation, be used as evidence of slow quenching.

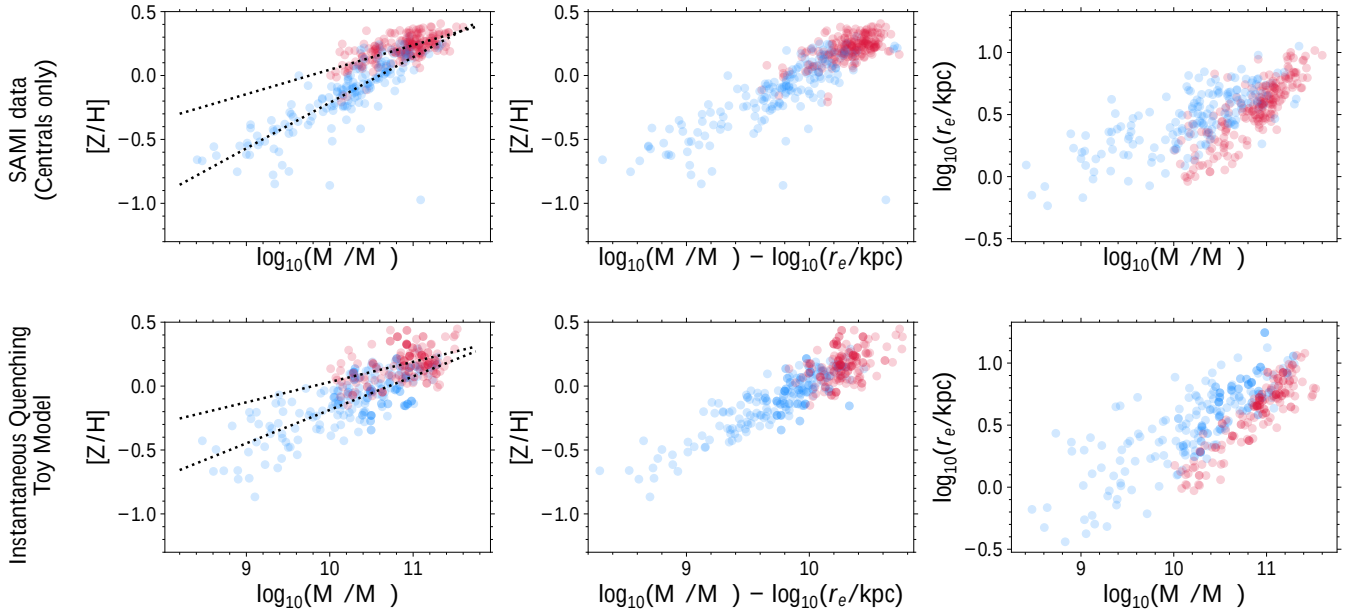

$$\delta R = 0.24\delta M_* \quad (7)$$

$$\delta[Z/H] = 0.45(\delta M_* - \delta R) \quad (8)$$

This evolution in [Z/H] as a function of gravitational potential comes from the slope of the potential-metallicity relation measured in Section 3, and the evolution in size as a function of mass matches that derived in Section 4.2.

The final piece is the inclusion of quenching. Figure 4 shows the mass-size plane of the galaxies in our central-only sample. A region containing the majority of the quenched galaxies in the sample is shown in grey. This region is bounded by three lines:

(i) $\log_{10}(M_*/M_\odot)$= 10, a line of constant stellar mass.
(ii) $\log_{10}(M_*/M_\odot)$- $2\log_{10}(r_e/\mathrm{kpc})$ = 9.7, a line of constant stellar surface density
(iii) $\log_{10}(M_*/M_\odot)$- $\log_{10}(r_e/\mathrm{kpc})$ = 10.25, a line of constant gravitational potential

In the model, if a galaxy grows in mass and size such that it crosses these lines and moves to the shaded region of the mass size plane, it is assigned a probability of quenching of $p_{\mathrm{quench}} = 0.1$. Galaxies outside the shaded region have $p_{\mathrm{quench}} = 0$.

At the start of each timestep, we draw a random number on the unit interval and compare with the above probability, p_{quench}, to decide whether a given galaxy continues to form stars or becomes quenched. If the galaxy quenches at a given timestep, it stops evolving completely in mass, size and metallicity; its values of these quantities at the onset of quenching are frozen in place until redshift zero. This model of galaxy quenching is effectively instantaneous (i.e. completely shutting down star-formation on a timescale of 100 Myrs), unlike the slow quenching (on timescales of Gyrs) discussed in P15 and T20. We note that our choice of $p_{\mathrm{quench}} = 0.1$ per timestep implies that a galaxy in the shaded region of the mass-size plane has a $\approx 70\%$ chance of quenching after 1 Gyr (10 timesteps).

We create 10^4 galaxies and evolve them forwards from their initial redshifts to today. We then compare quantitatively to the central-only SAMI sample discussed in Section 2, in order to minimise the effects of environmental quenching processes which are not included in our model. This reduces our sample of SAMI galaxies to 365. We then randomly sample 365 galaxies from our toy model with the same mass function as our SAMI galaxies. Finally, we add reasonable measurement uncertainties to our final model values; a 0.1 dex scatter in stellar mass and size and a 0.05 dex scatter in [Z/H].

Our results are shown in Figure 5. The top row shows the observed SAMI central galaxies and the bottom row shows results from our instantaneous quenching mode. We plot three important relationships: the mass-metallicity relation in the first column; the gravitational potential-metallicity relation in the second panel; and the mass-size relation in the third panel. Table 2 shows straight-line fits to the mass-metallicity and potential metallicity relations for both star-forming and quiescent galaxies in the model and the data, as well as fits to the quiescent galaxies in the mass-size plane.

We find that this very simple model can produce an offset in stellar metallicity between star-forming and quiescent galaxies at fixed mass, implying that slow quenching is not the only way to result in this. Our instantaneous quenching model recovers a difference of 0.17 dex between the metallicity of passive and star-forming galaxies at a mass of $\log_{10}(M_*/M_\odot)$= 10.5, identical to that from the central-only sample. The existence of this metallicity gap was used by P15 and T20 to conclude that most galaxies undergo slow quenching processes, but this work shows that such a gap can exist even when quenching is nearly instantaneous. Put simply, this is because the average low-redshift star-forming galaxy with a given stellar mass of M_* will *not* evolve into the average low-redshift passive galaxy with a stellar mass of M_*.

Table 2. A comparison of straight-line fits to the mass-metallicity, potential-metallicity and mass-size planes for the SAMI centrals and intantaneous quenching toy model shown in Figure 5. We fit a relation of the form $[Z/H] = m(\log_{10}(M_*/M_\odot) - 10.5) + c$ for the mass-metallicity relation; $[Z/H] = m(\log_{10}(\Phi/M_\odot kpc^{-1}) - 10) + c$ for the potential-metallicity relation; and $\log_{10}(r/kpc) = m(\log_{10}(M_*/M_\odot) - 10.5) + c$ for the mass-size relation.

	Gradient (m)		Intercept (c)	
	SAMI Centrals	Model	SAMI Centrals	Model
Mass-Metallicity (quenched)	0.19 ± 0.02	0.16 ± 0.03	0.14 ± 0.01	0.11 ± 0.01
Mass-Metallicity (SF)	0.36 ± 0.02	0.26 ± 0.02	-0.03 ± 0.01	-0.06 ± 0.01
Potential-Metallicity (quenched)	0.32 ± 0.03	0.36 ± 0.06	0.11 ± 0.01	0.07 ± 0.02
Potential-Metallicity (SF)	0.45 ± 0.03	0.47 ± 0.02	-0.03 ± 0.01	0.01 ± 0.01
Mass-Size (quenched)	0.58 ± 0.03	0.67 ± 0.03	0.33 ± 0.01	0.34 ± 0.01

We also quantitatively recover the location of quenched galaxies in the mass-size plane, and the behaviour of galaxies in the potential-metallicity plane from in Figure 2 and Section 3. The model also quite closely matches the slope of quiescent galaxies in the mass-size plane, as well as the slopes of quiescent and star-forming galaxies in the potential-metallicity plane.

We also note that the model does a good job of recovering the overall quenched fraction of galaxies, as well as the quenched fraction of galaxies as a function of mass. In this sample of SAMI centrals, 53% of galaxies are quenched, compared to the 42% of galaxies in our toy model which are quiescent. Figure 6 shows the distribution of quenched (red points) and star-forming (blue points) galaxies against stellar mass in the model (left panel) and in the SAMI data (middle panel). The black points show the fraction of galaxies that are quenched in mass bins of width 0.25 dex.

We also perform logistic regression on the SAMI galaxies and the model galaxies, using their stellar mass as an input. These are shown by the curved lines in each panel. Logistic regression uses the logistic function to model the binary outcome of whether a galaxy is still star-forming or quenched, and is simply another way to compare the quenched fractions as a function of mass between the model and the data. Both the binned fractions and logistic curves show that the model and the data agree well, although our model does slightly underpredict the fraction of galaxies which are quenched at $\log_{10}(M_*/M_\odot) > 10.5$.

4.3.1 Comparison with previous work

A number of previous studies have investigated quenching on populations of galaxies based on their evolution in M_* and r_e. These studies tend to fall into two categories: those which have galaxies evolving in the mass size plane before quenching at fixed velocity dispersion (or equivalently, gravitational potential, M_*/r_e), and those which find that galaxies quench at fixed surface density (M_*/r_e^2). van der Wel et al. (2009), Cappellari et al. (2013), van Dokkum et al. (2015) and Haines et al. (2017) can be broadly grouped into the former category, whilst Barro et al. (2017) and Tacchella et al. (2015) belong to the latter.

Chen et al. (2020) take this area modelling one step further and consider the evolution of galaxies in the four dimensional space of central surface density (Σ_1), M_*, r_e and central black hole mass, $M_\bullet$. Their work used a straight lines in the Σ_1-M_* plane which evolves with redshift as a quenching boundary, which they translated to the mass-size plane using the Sersic indices of quiescent galaxies. Their key insight is showing that this quenching boundary in the Σ_1-M_* plane can be related to the total energy deposited into the galaxy halo by the central black hole. Using such a model, Chen et al. (2020) recover an impressive number of correlations and properties of the galaxy population in the local Universe.

This study is the first to include stellar metallicity in a quenching model based on mass and size. In contrast to previous studies, we choose to use two different quenching boundaries in the mass-size plane: one at fixed gravitational potential and one at fixed surface density.

Using a boundary at fixed gravitational potential alone is unsatisfactory, since it tends to lead to a hard vertical line dividing quenched and star-forming galaxies in the [Z/H]-Φ plane. This is not observed in the data, where there is a small overlap between the two populations at $\Phi \approx 10.2$. We also find that a fixed Φ boundary leads to a steep slope in the [Z/H]-M_* plane for the quiescent galaxies, as well as too few quenched galaxies at low mass. This last point means that the quenched fractions as a function of mass in Figure 6 are not a good match. On the other hand, however, solely quenching as a function of surface density leads to too many low-mass quiescent centrals and a very flat slope in the [Z/H]-M_* plane. We therefore use a combination of the two to get the best match to our central-only sample.

We should stress that this exercise is designed to show that a sensible model using instantaneous quenching can be used to model galaxies in the [Z/H]-M_* plane, and to show that modelling stellar metallicities in this way can be accomplished by using the relationship between [Z/H] and gravitational potential. We do not aim to conclude that our quenching boundaries in Figure 4 supersede all others, or that this parameterisation of quenching should be taken as exactly what happens in the Universe. It is clear that the parameter space of possible such quenching models is very large, with the possibility of including time varying quenching boundaries, different functional forms of quenching probability (e.g. see Peng et al. 2010 and Lilly & Carollo 2016) and/or the inclusion of galaxy mergers and environmental-based quenching. Expanding our simple model in these ways is a topic for future work.

4.3.2 Implications

We find that our simple model of galaxy quenching which depends on both the mass and size of a galaxy can recover the difference in metallicity between star-forming and quiescent galaxies at fixed mass, implying that such a difference alone cannot be used as evidence of slow quenching processes. This is not to say that processes which remove a galaxy's halo of metal-poor gas are not important quenching pathways; evidence for disk strangulation (and its more extreme variant ram-pressure stripping) has been found in the local Universe (e.g. Poggianti et al. 2017; Owers et al. 2019), at higher redshifts (e.g. Maier et al. 2016, 2019; Vaughan et al. 2020) and in simulations (e.g. De Rossi et al. 2015).

Our model also implies that merging processes are not necessarily important in setting the slopes of the mass-size, [Z/H]-M_* and [Z/H]-Φ relations, since we recover these in a model that does not contain

Figure 6. The quenched fraction of galaxies in our toy model of quenching (left) and our sample of SAMI centrals (middle). We show whether galaxies are passive (red points, plotted at a y value around 1) or star-forming (blue points, at a y value around 0.0) as a function of their stellar mass. The points have had a small random jitter added such that they don't all lie on top of one another. Black points with error bars show the quenched fraction of galaxies in each bin of stellar mass. The curved lines show logistic regression fits to the same data. The right panel compares the logistic regression fits for the SAMI centrals (red) and the model galaxies (blue), showing the good agreement between the two.

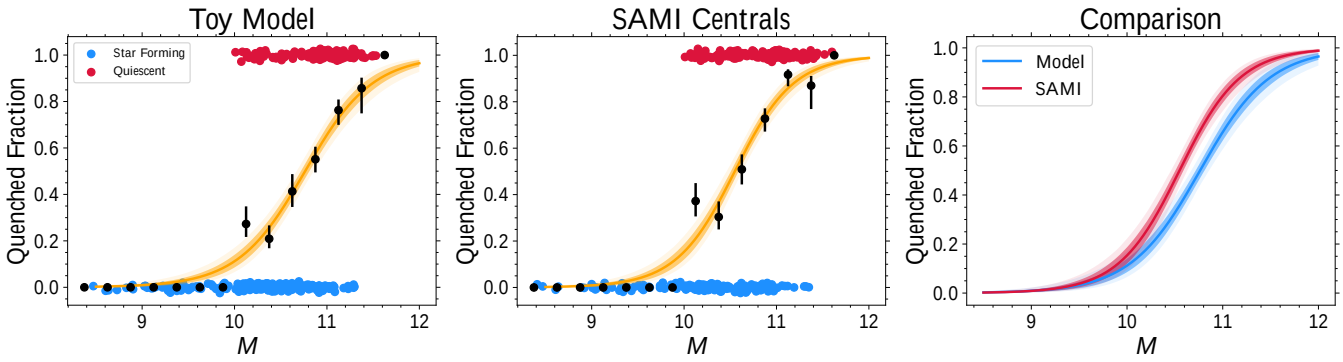

them. We do see a small differences in the intercept of the mass-size plane for quiescent galaxies, with our model containing objects which are ≈0.05 dex too small for their mass. Mergers would act to move objects towards the upper right of the mass-size plane, helping to close this gap.

The fact that our toy model of galaxy evolution recovers a number of important results without major mergers is perhaps not too surprising, since simulations have suggested that the rate of growth due to major mergers (mass ratio greater than 1:10) contribute only 20% of a galaxy's overall mass growth (Wang et al. 2011; L'Huillier et al. 2012). Whilst major mergers are more important in high-density environments, it is clear that accreting gas from the cosmic web is the predominant fuel source for most galaxies in the Universe.

5 CONCLUSIONS

This work builds on the studies of Barone et al. (2018), D'Eugenio et al. (2018) and Barone et al. (2020) by investigating the correlation between stellar metallicity ([Z/H]) and gravitational potential (Φ, derived from the photometric quantities M_* and r_e) for a homogeneously-observed sample of galaxies. We use the SAMI galaxy survey to measure central metallicity values for 1902 galaxies which also have robust stellar mass, half-light radius and star-formation rate measurements, and build a simply toy model of galaxy evolution which has galaxies evolving in mass, size and [Z/H] to explain our findings. Galaxies in this model have a probability p_q to undergo nearly instantaneous quenching (from main-sequence to fully passive in under 100 Myrs).

Our findings are as follows:

(i) We recover the well-known offset between the metallicity of star-forming and quiescent galaxies at fixed mass, with our results in very good agreement with the previous work of Peng et al. (2015) and Trussler et al. (2020).

(ii) We show for the first time that star-forming, passive and intermediate ("green valley") galaxies lie on the *same* [Z/H]-Φ relation, with passive galaxies preferentially being found at larger values of Φ.

(iii) The ability to predict [Z/H] from purely photometric quantities to an accuracy of 0.15 dex may be useful for large photometric surveys, providing an avenue to estimate stellar metallicities without spectroscopic observations.

(iv) We make the assumption that the slope of the [Z/H]-M_* and [Z/H]-Φ relations do not evolve with redshift and show that the gradients of the [Z/H]-M_* and [Z/H]-Φ relations imply a relationship between the rate of change of a galaxy's stellar mass with respect to its size. This relationship closely matches the slope of the mass-size plane for star-forming galaxies, but is a factor of ≈ 2 too shallow for passive galaxies. We take this as implying that star-forming galaxies evolve *along* the mass-size, [Z/H]-M_* and [Z/H]-Φ relations whilst accreting gas and forming new stars, but that the evolution of mass and size for quiescent galaxies is decoupled from their evolution in [Z/H].

(v) In our toy model of galaxy evolution, choosing a quenching probability which depends on a galaxy's mass *and size* allows us to quantitatively recover the slope of the [Z/H]-M_*, [Z/H]-Φ and mass-size relations for our sample, as well as account for the offset in metallicity between star-forming and passive galaxies at fixed mass. We therefore conclude that this offset is not necessarily the result of slow quenching, in contrast to the studies of Peng et al. (2015) and Trussler et al. (2020).

This study adds to the collection of work which shows the importance of accounting for galaxy size when investigating stellar populations, and not only considering stellar mass. Future work to investigate the [Z/H]-Φrelation of galaxies at higher redshifts (e.g in the forthcoming MAGPI survey; Foster et al. 2020), as well as in nearby low-mass galaxies and in cosmological simulations, will be invaluable to understand how fundamental it is to the evolution of galaxies in the Universe.

ACKNOWLEDGEMENTS

This research was conducted using the freely available Python programming language (Van Rossum & Drake Jr 1995) and the IPython extension (Perez & Granger 2007). Our analysis made use of the Numpy (van der Walt et al. 2011), Scipy (Virtanen et al. 2020), Astropy (Astropy Collaboration et al. 2013), matplotlib (Hunter 2007), and Pandas (Wes McKinney 2010) packages. We also use the Stan probabilistic programming language (Carpenter et al. 2017)

via its python extension, PYSTAN. We make extensive use of NASA's Astrophysics Data System.

The SAMI Galaxy Survey is based on observations made at the Anglo-Australian Telescope. The Sydney-AAO Multi-object Integral field spectrograph (SAMI) was developed jointly by the University of Sydney and the Australian Astronomical Observatory. The SAMI input catalogue is based on data taken from the Sloan Digital Sky Survey, the GAMA Survey and the VST ATLAS Survey. The SAMI Galaxy Survey is supported by the Australian Research Council Centre of Excellence for All Sky Astrophysics in 3 Dimensions (ASTRO 3D), through project number CE170100013, the Australian Research Council Centre of Excellence for All-sky Astrophysics (CAASTRO), through project number CE110001020, and other participating institutions. The SAMI Galaxy Survey website is http://sami-survey.org/.

We acknowledge the traditional custodians of the land on which the AAT stands, the Gamilaraay people, and pay our respects to their elders past, present and emerging.

DATA AVAILABILITY

The data underlying this article will be shared on reasonable request to the corresponding author.

REFERENCES

Abadi M. G., Moore B., Bower R. G., 1999, MNRAS, 308, 947
Abramson L. E., Gladders M. D., Dressler A., Oemler Augustus J., Poggianti B., Vulcani B., 2016, ApJ, 832, 7
Astropy Collaboration et al., 2013, A&A, 558, A33
Barone T. M., et al., 2018, ApJ, 856, 64
Barone T. M., D'Eugenio F., Colless M., Scott N., 2020, ApJ, 898, 62
Barro G., et al., 2017, ApJ, 840, 47
Bell E. F., de Jong R. S., 2001, ApJ, 550, 212
Bland-Hawthorn J., et al., 2011, Optics Express, 19, 2649
Blanton M. R., et al., 2017, AJ, 154, 28
Bryant J. J., O'Byrne J. W., Bland-Hawthorn J., Leon-Saval S. G., 2011, MNRAS, 415, 2173
Cappellari M., 2002, MNRAS, 333, 400
Cappellari M., 2016, ARA&A, 54, 597
Cappellari M., 2017, MNRAS, 466, 798
Cappellari M., Copin Y., 2003, MNRAS, 342, 345
Cappellari M., Emsellem E., 2004, PASP, 116, 138
Cappellari M., et al., 2013, MNRAS, 432, 1709
Carollo C. M., et al., 2013, ApJ, 773, 112
Carpenter B., et al., 2017, Journal of Statistical Software, 76
Cassata P., et al., 2013, ApJ, 775, 106
Chabrier G., 2003, PASP, 115, 763
Chen Z., et al., 2020, ApJ, 897, 102
Conroy C., 2013, ARA&A, 51, 393
Croom S. M., et al., 2012, MNRAS, 421, 872
Croom S. M., et al., 2021, MNRAS,
D'Eugenio F., Colless M., Groves B., Bian F., Barone T. M., 2018, MNRAS, 479, 1807
D'Eugenio F., et al., 2021, MNRAS,
Davidzon I., et al., 2017, A&A, 605, A70
De Rossi M. E., Theuns T., Font A. S., McCarthy I. G., 2015, MNRAS, 452, 486
Dekel A., Birnboim Y., 2006, MNRAS, 368, 2
Di Matteo T., Springel V., Hernquist L., 2005, Nature, 433, 604
Eisenstein D. J., et al., 2011, AJ, 142, 72
Eminian C., Kauffmann G., Charlot S., Wild V., Bruzual G., Rettura A., Loveday J., 2008, MNRAS, 384, 930
Foster C., et al., 2020, arXiv e-prints, p. arXiv:2011.13567
Franx M., Illingworth G., 1990, ApJ, 359, L41
Genel S., et al., 2018, MNRAS, 474, 3976
Graves G. J., Faber S. M., Schiavon R. P., 2009a, ApJ, 693, 486
Graves G. J., Faber S. M., Schiavon R. P., 2009b, ApJ, 698, 1590
Gunn J. E., Gott J. Richard I., 1972, ApJ, 176, 1
Haines C. P., et al., 2017, A&A, 605, A4
Hirschmann M., et al., 2013, MNRAS, 436, 2929
Hunter J. D., 2007, Computing In Science & Engineering, 9, 90
Kormendy J., Kennicutt Robert C. J., 2004, ARA&A, 42, 603
Krogager J. K., Zirm A. W., Toft S., Man A., Brammer G., 2014, ApJ, 797, 17
L'Huillier B., Combes F., Semelin B., 2012, A&A, 544, A68
Larson R. B., Tinsley B. M., Caldwell C. N., 1980, ApJ, 237, 692
Lee H.-c., Worthey G., Trager S. C., Faber S. M., 2007, ApJ, 664, 215
Lilly S. J., Carollo C. M., 2016, ApJ, 833, 1
Magorrian J., et al., 1998, AJ, 115, 2285
Maier C., et al., 2016, A&A, 590, A108
Maier C., Ziegler B. L., Haines C. P., Smith G. P., 2019, A&A, 621, A131
McDermid R. M., et al., 2015, MNRAS, 448, 3484
Medling A. M., et al., 2018, MNRAS, 475, 5194
Mowla L. A., et al., 2019, ApJ, 880, 57
Naab T., Johansson P. H., Ostriker J. P., 2009, ApJ, 699, L178
Nelan J. E., Smith R. J., Hudson M. J., Wegner G. A., Lucey J. R., Moore S. A. W., Quinney S. J., Suntzeff N. B., 2005, ApJ, 632, 137
Noeske K. G., et al., 2007, ApJ, 660, L43
Oser L., Ostriker J. P., Naab T., Johansson P. H., Burkert A., 2010, ApJ, 725, 2312
Owers M. S., et al., 2019, ApJ, 873, 52
Peng Y.-j., et al., 2010, ApJ, 721, 193
Peng Y., Maiolino R., Cochrane R., 2015, Nature, 521, 192
Perez F., Granger B. E., 2007, Computing in Science Engineering, 9, 21
Poggianti B. M., et al., 2017, ApJ, 844, 48
Renzini A., Peng Y.-j., 2015, ApJ, 801, L29
Robotham A. S. G., et al., 2011, MNRAS, 416, 2640
Schawinski K., et al., 2014, MNRAS, 440, 889
Scott N., et al., 2009, MNRAS, 398, 1835
Scott N., et al., 2017, MNRAS, 472, 2833
Sellwood J. A., 2014, Reviews of Modern Physics, 86, 1
Sharp R., et al., 2006, in McLean I. S., Iye M., eds, Society of Photo-Optical Instrumentation Engineers (SPIE) Conference Series Vol. 6269, Society of Photo-Optical Instrumentation Engineers (SPIE) Conference Series. p. 62690G (arXiv:astro-ph/0606137), doi:10.1117/12.671022
Silk J., Rees M. J., 1998, A&A, 331, L1
Skelton R. E., et al., 2014, ApJS, 214, 24
Speagle J. S., Steinhardt C. L., Capak P. L., Silverman J. D., 2014, ApJS, 214, 15
Tacchella S., et al., 2015, Science, 348, 314
Taylor E. N., et al., 2011, MNRAS, 418, 1587
Thomas D., Maraston C., Bender R., Mendes de Oliveira C., 2005, ApJ, 621, 673
Tinsley B. M., 1968, ApJ, 151, 547
Trager S. C., Faber S. M., Worthey G., González J. J., 2000, AJ, 120, 165
Trussler J., Maiolino R., Maraston C., Peng Y., Thomas D., Goddard D., Lian J., 2020, MNRAS, 491, 5406
Van Rossum G., Drake Jr F. L., 1995, Python reference manual. Centrum voor Wiskunde en Informatica Amsterdam
Vaughan S. P., et al., 2020, MNRAS, 496, 3841
Vazdekis A., et al., 2015, MNRAS, 449, 1177
Virtanen P., et al., 2020, Nature Methods, 17, 261
Wang J., et al., 2011, MNRAS, 413, 1373
Wes McKinney 2010, in Stéfan van der Walt Jarrod Millman eds, Proceedings of the 9th Python in Science Conference. pp 56 – 61, doi:10.25080/Majora-92bf1922-00a
Woo J., Ellison S. L., 2019, MNRAS, 487, 1927
Woo J., Carollo C. M., Faber S. M., Dekel A., Tacchella S., 2017, MNRAS, 464, 1077
York D. G., et al., 2000, AJ, 120, 1579
Zolotov A., et al., 2015, MNRAS, 450, 2327

van Dokkum P. G., et al., 2010, ApJ, 709, 1018
van Dokkum P. G., et al., 2013, ApJ, 771, L35
van Dokkum P. G., et al., 2015, ApJ, 813, 23
van der Walt S., Colbert S. C., Varoquaux G., 2011, Computing in Science Engineering, 13, 22
van der Wel A., Bell E. F., van den Bosch F. C., Gallazzi A., Rix H.-W., 2009, ApJ, 698, 1232
van der Wel A., et al., 2014, ApJ, 788, 28

This paper has been typeset from a TEX/LATEX file prepared by the author.